RESEARCH ARTICLE

NANO · MICRO small
www.small-journal.com

Evolving Emulsion Microcompartments via Enzyme-Mimicking Amyloid-Mediated Interfacial Catalysis

Peiyong Song, Jing Chen, Dan Zhao, Ke Shi, Runze Xu, Mengyue Zhu, Li Zhao, E. Thomas Pashuck, Liliang Ouyang, Fang Jiao, and Yiyang Lin**

Living organisms take in matter and energy from their surroundings, transforming these inputs into forms that cells can use to sustain metabolism and power various functions. A significant advancement in the development of protocells and life-like materials has been the creation of cell-like microcompartments capable of evolving into higher-order structures characterized by hierarchy and complexity. In this study, a smart emulsion system is designed to digests chemical substrates and generates organic or inorganic products, driving the self-organization and structuration of microcompartments. Central to this system is a lipase-derived peptide that undergoes amyloid fibrillation, exhibiting hydrolase-like activity and stabilizing Pickering emulsions. Through catalytic hydrolysis or silicatein-inspired mineralization, these emulsion microcompartments generate self-organized surfactant layers from organic substrates or silica scaffolds from inorganic substrates at the oil–water interface, respectively, helping to prevent coalescence. This process further facilitates a structural evolution into high-internal phase emulsion gels that are suitable for direct-ink-writing 3D printing. The findings underscore the potential for designing self-evolving soft materials that replicate the structures and functions of living organisms.

1. Introduction

Living organisms sustain life through a series of complex, interrelated processes that enable growth, reproduction, and the maintenance of homeostasis.[1] Central to these processes is the ability of cells to convert nutrients, particularly glucose, into energy in the form of adenosine triphosphate, which is used to build materials and power various functions. This remarkable feature has inspired research into the development of self-organizing soft materials as cell mimics.[2] For instance, compartmentalized cell-like structures have been created in the form of vesicles, polymersomes, colloidosomes, proteinosomes, emulsions, and coacervates.[3] These synthetic compartments replicate fundamental cellular features and biological processes, such as multicompartmentalization,[4] mediating biochemical reaction,[5] transmembrane signaling,[6] and cellular communication.[7] In biology, cells develop and differentiate to acquire specialized forms and functions. Additionally, living organisms have evolved cell-mediated biomineralization mechanisms to construct structurally ordered, environmentally adaptive composite materials.[8] In this context, the construction of soft materials that can improve and evolve into more complex structures through biomimetic processes represents a crucial step toward the replication of living systems, offering a tool to develop intelligent materials.[9]

In this work, we sought to construct bio-inspired materials capable of evolving into higher-order structures or transforming

P. Song, J. Chen, K. Shi, M. Zhu, Y. Lin
State Key Laboratory of Chemical Resource Engineering
Key Lab of Biomedical Materials of Natural Macromolecules (Beijing University of Chemical Technology
Ministry of Education)
Beijing Laboratory of Biomedical Materials
Beijing University of Chemical Technology
Beijing 100029, China
E-mail: y.lin@mail.buct.edu.cn

D. Zhao, F. Jiao
Laboratory of Soft Matter Physics
Institute of Physics
Chinese Academy of Sciences
Beijing 100190, China

R. Xu, L. Ouyang
Department of Mechanical Engineering
Tsinghua University
Beijing 100084, China

L. Zhao
School of Light Industry
Beijing Technology & Business University (BTBU)
Beijing 100048, China
E-mail: zhaol@btbu.edu.cn

E. T. Pashuck
Department of Bioengineering
Lehigh University
Bethlehem, PA 18015, USA

The ORCID identification number(s) for the author(s) of this article can be found under https://doi.org/10.1002/smll.202409601

DOI: 10.1002/smll.202409601

into different forms.[10] This was accomplished by creating cell-sized Pickering emulsion microcompartments stabilized by catalytically active amyloid nanofibrils, which were assembled from a lipase-derived tridecapeptide. A Pickering emulsion is a type of emulsion stabilized by colloidal particles that adsorb strongly at the oil–water interface, preventing the coalescence of dispersed droplets and enhancing emulsion stability. Unlike conventional surfactant-stabilized emulsions, Pickering emulsions offer several advantages, including high stability, reduced toxicity, and the potential for stimuli-responsive behavior. These properties make Pickering emulsions highly desirable for applications in fields such as biomedicine, food science, and material engineering. Driven by multiple non-covalent interactions, bio-inspired peptides self-assemble into highly ordered, insoluble fibrillar aggregates called amyloid fibrils. These fibrils are characterized by a distinct cross-β-sheet structure, where β-strands run perpendicular to the fibril axis, forming a stable, stacked arrangement.[11] The amphiphilic nature and micron-scale size of the amyloid nanofibrils promote their adsorption at the oil–water interface, effectively reducing interfacial tension and enhancing the stability and robustness of the emulsion microcompartments.[12] Additionally, amyloid fibrils offer attractive sequence-specific properties, including catalytic activity, bioactivity, and stimuli-responsiveness, making them promising candidates for the preparation of functional emulsions. The dynamic feature of supramolecular fibrillation endowed the design of smart emulsions, in which emulsification/demulsification was dependent on the fibrillation states and solution pH.[13] Herein, with amyloid fibrils acting as artificial enzymes at the oil–water interface, the emulsion microcompartments exhibited self-evolving and self-strengthening behaviors by forming a self-organized surfactant layer at the interface, resulting in solid-like films. Notably, the interfacial catalytic reaction also induced phase inversion of the Pickering emulsion, driving the formation of high-internal phase emulsion (HIPE) gels.[14] Additionally, the emulsion system catalyzed hydrolysis-condensation of alkoxysilane and thereby generated a silica scaffold at the interface via a silicatein-inspired biomineralization mechanism, leading to emulsion solidification.

2. Results and Discussion

2.1. Design Principle of Self-Evolving Emulsion Microcompartments

Emulsification is a widely used technique that creates compartmentalized systems. In these systems, small droplets are dispersed within a continuous phase, and the interface between the droplets and the continuous phase is stabilized using surfactants, peptides, proteins, polymers, or particles.[15] In the absence of stabilizers, emulsion droplets are prone to coalescence or Ostwald ripening, resulting in macroscopic phase separation.[16] In this study, we designed a Pickering emulsion system stabilized by amyloid-like nanofibrils, which reduced the interfacial tension and stabilize oil-in-water emulsions. The emulsions were able to transform into higher-order emulsion microcompartments with improved stability via two biomimetic mechanisms (**Figure** 1a,b). In Pathway I, supramolecular nanofibrils demonstrated lipase-like activity, promoting the hydrolysis of ester substrates and forming a self-organized surfactant layer at the oil–water interface. This process ultimately led to the self-reinforcement and structural evolution into HIPE gels. In Pathway II, the supramolecular nanofibrils exhibited silicatein-like activity, facilitating biomimetic silicification and creating a biomineralized interfacial scaffold to enhance compartment robustness.

To achieve these, we designed a β-sheet tridecapeptide derived from *Aspergillus flavus* lipase with the amino acid sequence KIVVVGHSLGAAI (denoted as KIV). This peptide featured a positively charged lysine at N-terminus, a catalytic Gly-His-Ser, and a β-sheet forming sequence (IVVV) (Figure 1c and S1, Supporting Information). In biochemistry, lipase catalyzes the hydrolysis of a wide range of substrates, including esters of cholesterol and phospholipids, with the histidine residue playing a key role in catalyzing ester bond hydrolysis through an electrophilic reaction.[17] Driven by its β-sheet structure, the KIV tridecapeptide underwent amyloid fibrillation in aqueous solution through a process involving nucleation, propagation, and elongation.[18] We determined the critical aggregation concentration (CAC) of KIV to be 0.12 mM using Thioflavin T (ThT) and Nile red as fluorescence probes, in which the former recognized the β-sheet stacking and the latter detected the existence of hydrophobic domain (Figure S2, Supporting Information). Atomic force microscopy (AFM) confirmed the spontaneous formation of micron-long amyloid nanofibrils when the concentration exceeded CAC (Figure 1d,e), with a twisted pattern along the fibril axis and a periodicity of ≈39 nm. The height distribution of the KIV nanofibrils was analyzed, and a Gaussian fitting revealed a well-defined distribution of nanofibril thickness of ≈5.5 nm (Figure S3, Supporting Information). Transmission electron microscopy (TEM) further confirmed the formation of supramolecular nanofibrils several micrometers in length (Figure S4, Supporting Information). At higher concentrations, KIV nanofibrils formed entangled 3D networks, leading to hydrogelation (Figure S5, Supporting Information). Circular dichroism (CD) analysis showed a typical β-sheet conformation with a negative peak at 216 nm (Figure 1f), which intensified as the concentration exceeded 0.15 mM, in agreement with the ThT and Nile red fluorescence measurement (Figure S6, Supporting Information).

Supramolecular self-assembly of designer peptides has been extensively explored to mimic the complex arrangement of catalytically active residues in enzymes.[19] Given that KIV was derived from the active site of lipase, we set out to examine the hydrolase-mimicking property of the resulting amyloid nanofibrils. For this, we used 1-propyl pyrene-3,6,8-trisulfonate (PrPTS) as a fluorogenic substrate, which underwent accelerated hydrolysis in the presence of histidine-containing peptide.[6,20] Through imidazole-mediated nucleophilic reaction, PrPTS was hydrolyzed into HPTS, which emitted a strong green fluorescence (Figure 1g and S7, Supporting Information). To further assess the catalytic activity of the amyloid-like nanofibrils, we used p-nitrophenyl acetate (PNPA) as a chromogenic substrate, which was hydrolyzed into p-nitrophenol (PNP) (Figure S7 and Table S1, Supporting Information). Notably, the KIV nanofibrils were demonstrated with higher catalytic activity compared to the non-aggregated KIV (Figure S8, Supporting Information).

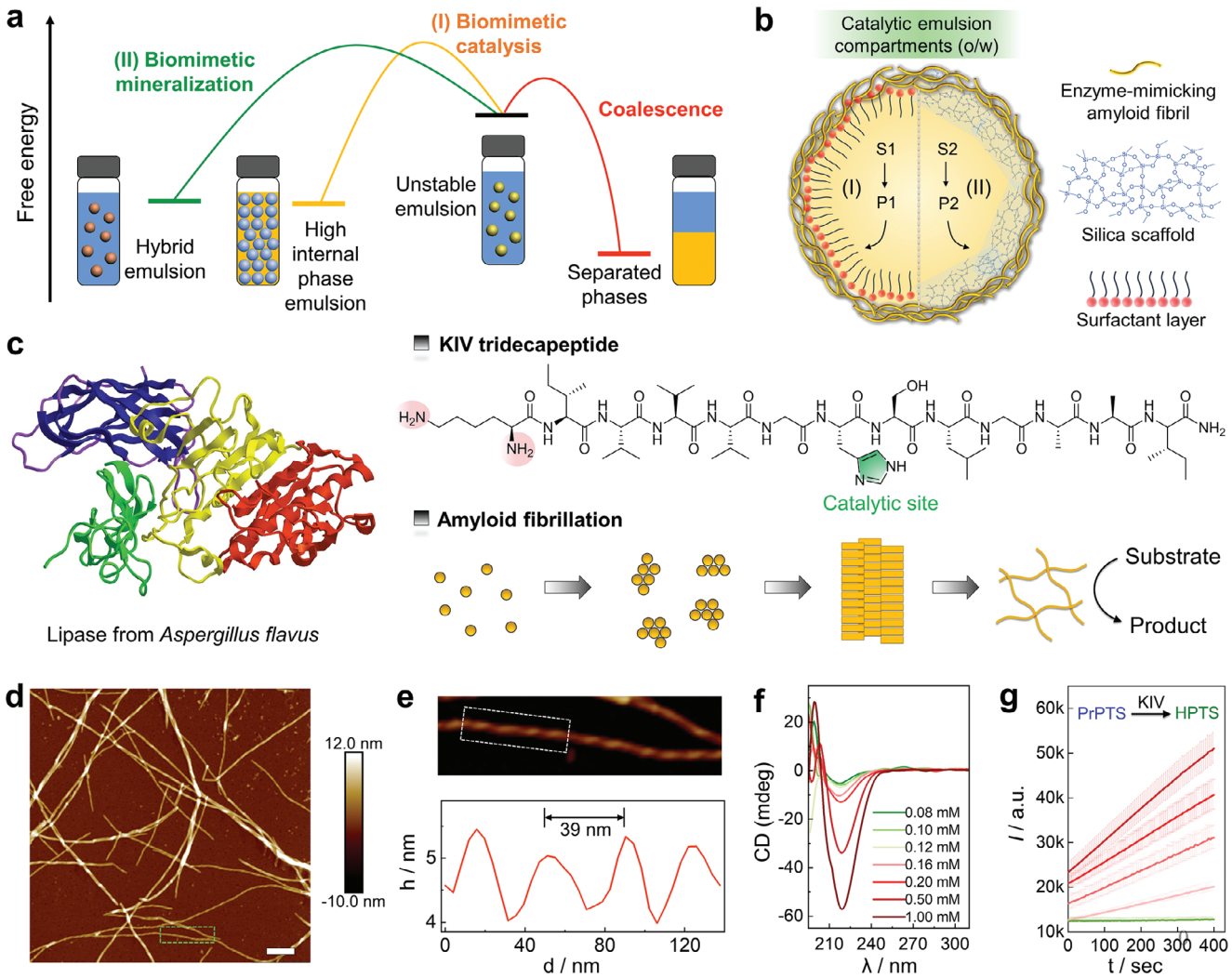

Figure 1. Design principle of self-evolving emulsion microcompartments. a) Free energy landscape and thermodynamic stability of oil-in-water (o/w) Pickering emulsion, which evolved into a stable emulsion with increased complexity via two biomimetic mechanisms. Pathway I: the o/w emulsion droplets experienced phase inversion and transformed into HIPE gels through a biocatalytic reaction mechanism, resulting in the formation of. Pathway II: silica networks were generated at the oil–water interface via a biomineralization mechanism. b) The o/w Pickering emulsion was stabilized by the interfacial assembly of amyloid nanofibrils, which further catalyzed the hydrolysis of substrates to generate a self-organized surfactant layer that binds to nanofibrils, or form silica networks at the interface. c) The 3D structure of lipase from *Aspergillus flavus* and a 13-amino acid fragment (KIVVVGH-SLGAAI, denoted KIV) derived from lipase. The histidine residue on KIV played a key role in catalyzing substrate hydrolysis, while the β-sheet forming sequences drove fibrillation through a nucleation-oligomerization-maturation process. d,e) Atomic force microscopy (AFM) images showed the formation of supramolecular nanofibrils (d) and an enlarged image of a helical nanofibril (e). The corresponding height profile indicated by the dashed rectangle revealed a periodic height change along the long axis of the nanofibril. Scale bar in (d) 100 nm. f) Circular dichroism (CD) spectra of KIV solutions, show an intensified negative maximum at 216 nm, confirming the formation of β-sheet secondary structures. g) Kinetic study of KIV-catalyzed hydrolysis of 1-propyl pyrene-3,6,8-trisulfonate (PrPTS), tracking fluorescence emission from the product 8-hydroxy-1,3,6-pyrenetrisulfonic acid trisodium (HPTS, $\lambda_{ex} = 480$ nm, $\lambda_{em} = 520$ nm). KIV concentrations were 0, 0.1, 0.2, 0.3, and 0.5 mM (from bottom to top). Data represent mean ± s.d. of three replicates.

2.2. Amyloid Nanofibril as Emulsifier

The KIV nanofibrils were subsequently utilized as stabilizing agents for the preparation of Pickering emulsions. To achieve this, an aqueous solution containing KIV nanofibrils was mixed with a specific amount of organic solvent, followed by mechanical homogenization to generate a microemulsion. Pickering emulsion was typically formed using a chloroform/water (3:7) mixture, with the top phase being a clear aqueous solution and the bottom phase containing a pale white Pickering emulsion (**Figure 2a**). In these systems, Nile red, a lipophilic stain, was distributed in the inner pool, and HPTS, which electrostatically stains the KIV nanofibrils, absorbed at the interface. This suggested the formation of chloroform-in-water emulsion with the assembly of KIV nanofibrils at the oil–water interface. As the concentration of the KIV concentration increased, the diameter of the emulsion droplets decreased, from 28 μm at 0.5 mM to 15 μm at 1.0 mM, 12 μm at 1.5 mM, and 10 μm at 2.0 mM (Figure 2b and S9, Supporting Information). This reduction in droplet size was attributed to the higher concentrations of nanofibrils, which

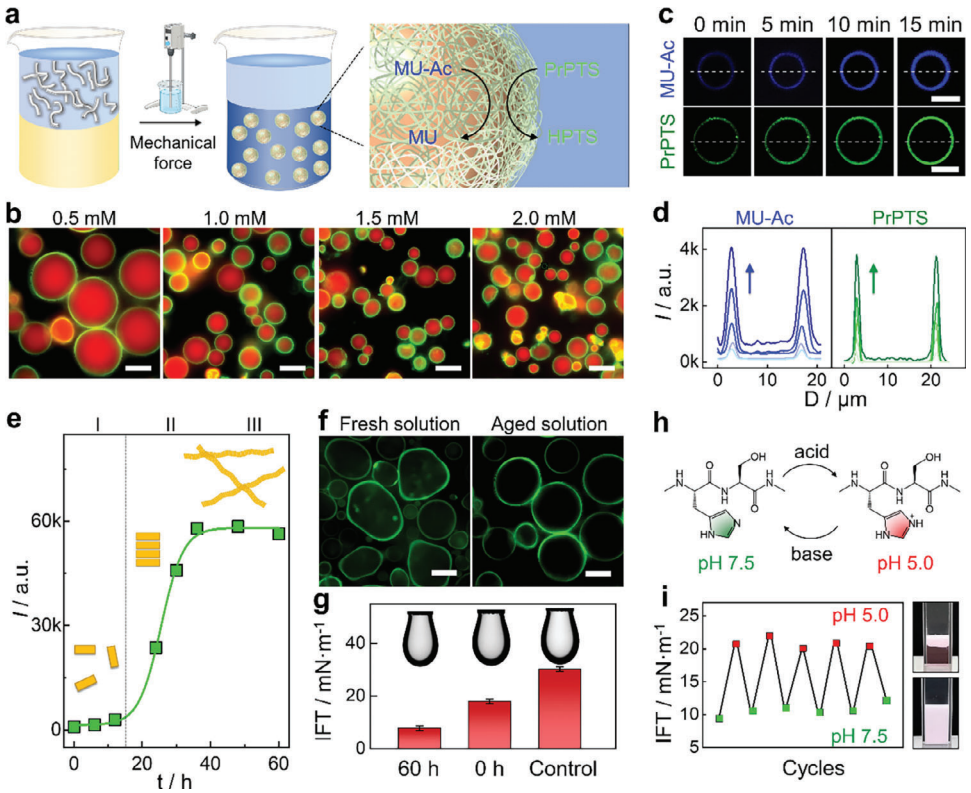

Figure 2. Interfacial assembly of amyloid-like nanofibrils for stabilizing Pickering emulsions. a) Schematic illustration and b) fluorescence microscopy images showing the formation of KIV nanofibril-stabilized chloroform-in-water Pickering emulsion with varied KIV concentrations. The organic phase was stained with Nile red, while the KIV fibrils at the o/w interface were electrostatically stained with HPTS. c) Time-lapse fluorescence microscopy images depicting the hydrolysis of 1-propyl pyrene-3,6,8-trisulfonate (PrPTS in aqueous phase) and 4-methylumbelliferyl acetate (MU-Ac in organic phase). These substrates were converted to HPTS (green) and 4-methylumbelliferone (MU, blue), respectively, which were primarily bound to the amyloid fibrils at the interface. d) Time-dependent fluorescence intensity (*I*) profile along the dashed line across the emulsion droplet, showing a continuous increase in fluorescence as the catalyzed hydrolysis reaction progressed. e) Time-dependent ThT fluorescence (*I*) tracing amyloid fibrillation in KIV solution, where nucleation occurred during the lag phase (Phase I) and was followed by oligomerization (Phase II), leading to the formation of mature nanofibrils (Phase III). f) Fluorescence microscopy images of emulsion droplets (stained with HPTS), stabilized with fresh (0 h) and aged (60 h) KIV solution at pH 7.5. g) Comparison of chloroform–water interface tension (IFT) in the presence of fresh KIV solution (0 h) and mature KIV nanofibrils (60 h), and a control without KIV. Mature nanofibrils demonstrated a greater ability to lower interface tension. h) pH-dependent protonation and deprotonation of imidazole group on the histidine residue of KIV. i) Left: variation in interfacial tension at the chloroform/water interface with repeated changes in the pH of the aqueous solution. Right: The Pickering emulsion displayed greater stability at pH 7.5, whereas at pH 5.0, the emulsion underwent phase separation. Scale bars: (b,f) 20 μm; (c) 10 μm.

more effectively prevent coalescence of the emulsion microdroplets, thus stabilizing smaller droplets. The Pickering emulsion was prepared across a wide range of chloroform/water ratios (Figure S10, Supporting Information) and exhibited long-term stability (Figure S11, Supporting Information).

The formation of Pickering emulsions stabilized by amyloid nanofibrils was further demonstrated with a variety of organic solvents (e.g., butanol, dichloromethane, dichloroethane, chloroform, ethyl ester, *tert*-Butyl methyl ether, toluene, hexane and heptane) (Figure S12, Supporting Information). In all cases, two distinct phases were observed: a dilute aqueous phase and a Pickering emulsion phase. For solvents denser than water, such as chloroform and dichloromethane, the Pickering emulsion was located in the bottom phase. Conversely, for less dense solvents, the Pickering emulsion formed in the top phase (Figure S13, Supporting Information). Moreover, w/o emulsions were obtained with organic solvents (e.g., hexanol, 2-ethyl-1-hexanol, and n-decanol) having higher $E_T(30)$ solvent polarity values, while o/w Pickering emulsions were formed in solvents with lower $E_T(30)$ solvent polarity values. The catalytic activity of amyloid nanofibrils at the oil–water interface was demonstrated by the hydrolysis of both the hydrophobic substrate 4-methylumbelliferyl acetate (MU-Ac) into 4-methylumbelliferone (MU, blue fluorescent) and the hydrophilic substrate PrPTS into HPTS (green fluorescent). (Figure 2c,d and S7, Supporting Information).

Compared to conventional emulsions stabilized by surfactants and polymers, Pickering emulsions stabilized by colloid particles are usually much more stable, where particles adsorb at the oil–water interface forming a solid particle layer preventing coalescence.[21] We reasoned that the fibrillation state of tridecapeptide could significantly impact the stability of the Pickering emulsion. Amyloid fibrillation typically involves three stages: a lag phase (Phase I), an elongation phase (Phase II), and a mature phase (Phase III), as indicated by ThT fluorescence, corresponding to nucleation, oligomerization, and fibrillation (Figure 2e). To test this, we prepared a fresh KIV solution (0 h incubation)

and a KIV solution aged for 60 h for emulsification. The fresh solution exhibited low ThT fluorescence (Figure 2e) and CD intensity at 216 nm (Figure S14, Supporting Information), indicating the absence of well-formed β-sheet structures and nanofibrils. By contrast, the aged KIV solution exhibited strong ThT fluorescence and CD intensity, confirming the formation of β-sheets that drove fibrillation. Notably, the fresh KIV solution in the nucleation stage displayed limited capability to stabilize the Pickering emulsion, as evidenced by the coalescence of the emulsion droplets and their irregular shapes (Figure 2f). In contrast, Pickering emulsions prepared with the aged KIV solution remained stable. In summary, micron-long mature nanofibrils functioned as amphiphilic particles, reducing oil–water interface tension and stabilizing the emulsion droplets. Moreover, both fresh and aged KIV solutions (c = 0.5 mM) reduced the chloroform–water interfacial tension from 30.15 to 17.93 and 7.73 mN m^{-1}, respectively, where the mature nanofibrils exhibited a higher interface activity (Figure 2g).

The imidazole group on histidine has a pK_a of ≈6.6, allowing for protonation in acidic conditions and deprotonation in basic conditions (Figure 2h). This property enabled facile control over the emulsification and demulsification by adjusting the solution pH. At pH 7.5, the imidazole group was deprotonated, favoring the amyloid fibrillation of KIV. The assembly of elongated amyloid nanofibrils at the chloroform–water interface reduced the interfacial tension (30.15 to 7.73 mN m^{-1}) and enhanced the stability of the Pickering emulsion. Conversely, at pH 5.0, the imidazole group was mostly protonated, increasing the peptide hydrophilicity and lowering the propensity of KIV fibrillation, as confirmed by CD and ThT analysis (Figure S15, Supporting Information). As a result, non-aggregated KIV was less effective at stabilizing the Pickering emulsion under acidic conditions (Figure 2i and S16, Supporting Information). Remarkably, when the pH was raised back to 7.5, re-emulsification of the chloroform–water mixture occurred. This process can be cycled repeatedly by alternately adding HCl and NaOH (Figure 2i and S17, Supporting Information).

2.3. Biomimetic Catalysis-Fueled Emulsion Evolution

Having demonstrated that KIV nanofibrils exhibited hydrolase-like properties and were capable of stabilizing Pickering emulsion, we sought to harness biomimetic catalysis to drive the evolution of emulsion materials (**Figure 3a**). In our design, a series of *p*-nitrophenyl esters (substrates) were loaded in the oil phase of chloroform/water Pickering emulsion, where they were hydrolyzed into 4-nitrophenol and fatty acid, catalyzed by KIV nanofibrils at the interface. In this reaction, histidine, commonly found in the active sites of esterases and lipases, is expected to facilitate nucleophilic catalysis.[22] Notably, supramolecular self-assembly was demonstrated to generate reactive microenvironments that effectively attracted and bound the substrate. In our system, the resulting fatty acids, acting as anionic surfactants, self-organized at the oil–water interface by electrostatic interactions with lysine residues on KIV, further enhancing the interfacial stability of the emulsion.

To test our hypothesis, we evaluated the catalytic hydrolysis of p-nitrophenyl ester in the presence of KIV nanofibrils (Figure S18, Supporting Information). The hydrolysis of p-nitrophenyl laurate rapidly reduced the chloroform–water interfacial tension, which reached equilibrium within 40, 50, and 85 s, when the substrate concentration was 0.5, 1.0, and 2.0 mM, respectively (Figure 3b). Moreover, p-nitrophenyl esters with longer alkyl chains more efficiently reduced interfacial tension from 18 mN m^{-1} for n = 0 to 8 mN m^{-1} for n = 16 (Figure 3c, [KIV] = 0.2 mM). The impact of ester hydrolysis was further investigated using a pendent droplet method in jammed and unjammed states,[23] in which a droplet of chloroform containing p-nitrophenyl laurate (n = 10) was immersed in an aqueous solution of KIV nanofibrils (Figure 3d, top). When the droplet volume was reduced to compress the interfacial assembly, wrinkles appeared on the droplet surface, indicating that amyloid fibrils had jammed at the interface. This jamming reduced the mobility of the KIV nanofibrils, causing them to exhibit solid-like characteristics (Figure 3d, top). When the droplet volume was expanded, the solid-like film could relax. Without ester substrates in the chloroform droplet, no wrinkles were observed under compression, suggesting that the binding energy of KIV nanofibrils was insufficient to stabilize the interface (Figure 3d, bottom). To further assess the effect of ester hydrolysis on Pickering emulsion stability, a chloroform/water Pickering emulsion was prepared at a low KIV concentration (0.2 mM) with p-nitrophenyl esters incorporated into the oil phase. Without substrates, the emulsion destabilized over time, with droplet coalescence leading to macroscopic phase separation. This instability persisted when ester substrates had shorter alkyl chains (n < 10) (Figure 3e,f). However, in the presence of substrates with longer hydrophobic chains (n ≥ 10), the emulsion droplets remained stable, preventing coalescence and maintaining emulsification. In the process of substrate hydrolysis, no structural or morphological changes were noticed for the emulsion droplets (Figure S19, Supporting Information). We attributed the above results to the cooperative complexation between amyloid fibrils and fatty acids. The binding of fatty acids reduced the electrostatic repulsion between amyloid fibrils, which originated from protonated lysine side groups, leading to a more closely packed of amyloid nanofibrils. Additionally, the absorption of fatty acids contributed to a reduction in interfacial tension and a decrease in the mobility of amyloid fibrils.

Particle adsorption at the oil–water interface is significantly influenced by wettability, which is characterized by the three-phase contact angle (θ). According to the empirical Finkle rule, the emulsion type (o/w or w/o) is directly correlated with θ (**Figure 4a**). Hydrophilic particles with $\theta < 90°$ are less wetted by the oil phase, forming an o/w Pickering emulsion. By contrast, hydrophobic particles ($\theta > 90°$) are better wetted by the oil phase, forming a w/o Pickering emulsion. In our system, histidine-mediated interfacial catalysis produced a fatty acid that self-organized at the interface by binding to amyloid nanofibrils, contributing to the increase in the hydrophobicity of the nanofibril particles, and thereby affecting θ (Figure 4b). Additionally, the electrostatic binding of fatty acids at the interface caused a more close packing of amyloid nanofibrils. We hypothesize that these changes eventually drive the phase inversion of o/w emulsion into stable w/o emulsion. To test this hypothesis, we prepared a chloroform-in-water (25:75) Pickering emulsion using mature KIV nanofibrils as the stabling agent, loading p-nitrophenyl

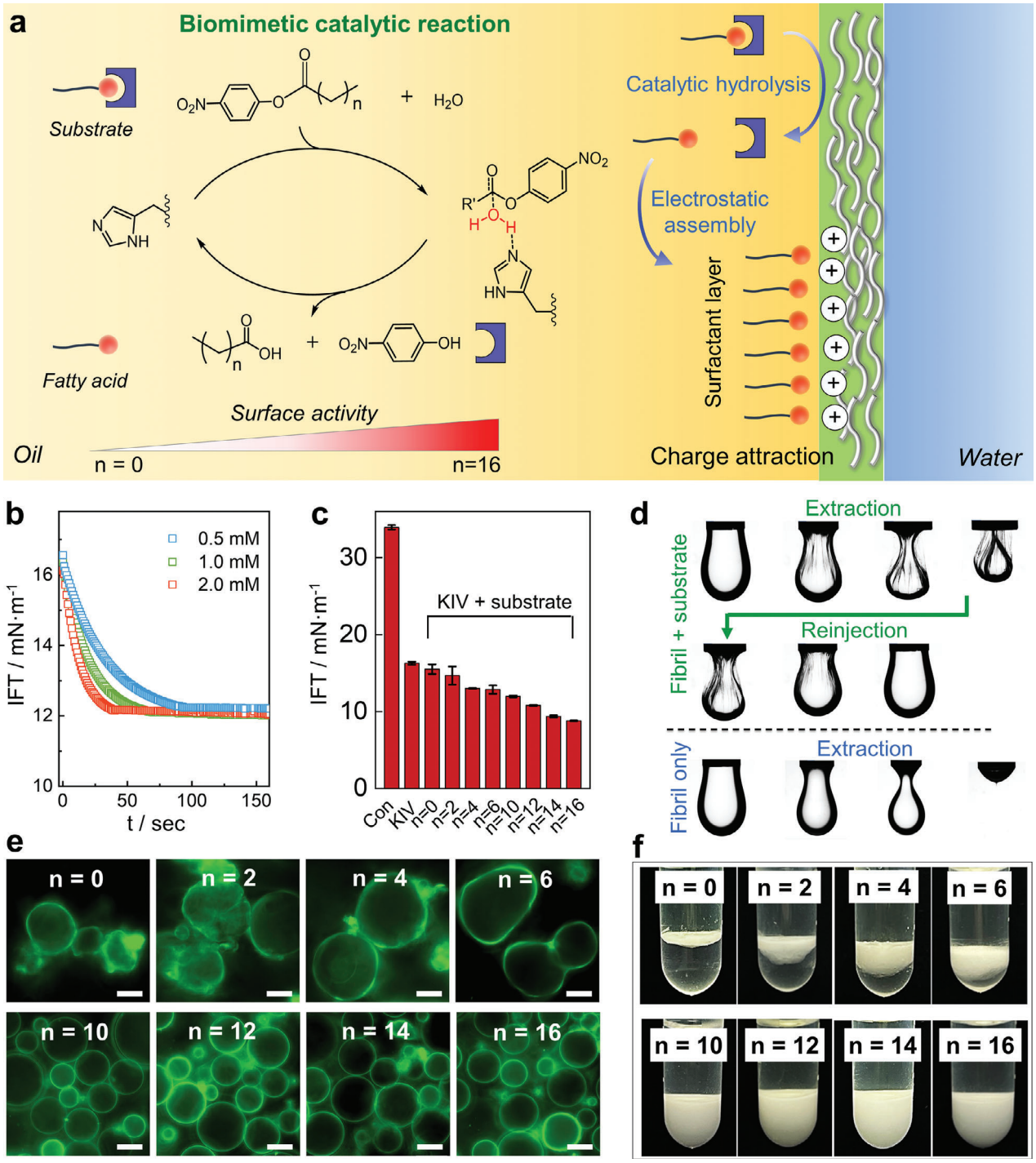

Figure 3. Self-reinforcement of emulsion microcompartments through interfacial catalysis. a) Schematic illustration of the biomimetic catalytic reaction enhancing emulsion stability. The histidine residue on KIV catalyzed the hydrolysis of p-nitrophenol esters into aliphatic acids and p-nitrophenol. Increasing the length of alkyl tails enhanced the interfacial activity of fatty acids, which electrostatically bound to the lysine residue of KIV, thereby increasing the interfacial stability of the emulsion. The fatty acid produced included acetic acid (n = 0), butanoic acid (n = 2), hexanoic acid (n = 4), octanoic acid (n = 6), dodecanoic acid (n = 10), myristic acid (n = 12), palmitic acid (n = 14) and stearic acid (n = 16). b) Time-varied chloroform–water interfacial tension in the process of catalytic hydrolysis, where nitrophenol ester (n = 10, 0.5, 1.0, and 2.0 mM) was loaded into the oil phase and the KIV concentration in the aqueous phase was 0.2 mM. c) The interfacial tension at the chloroform–water interface was lowered in the presence of KIV (0.2 mM) and p-nitrophenol esters (n = 0–16, 1.0 mM). d) Snapshots illustrating the evolution of a chloroform droplet in an aqueous environment containing amyloid fibrils during an extraction–reinjection process. Line 1 and 2: the aqueous phase contained KIV nanofibrils (0.5 mM) and the chloroform phase contained substrate (n = 10, 5 mM). Line 3: the aqueous phase was loaded with KIV nanofibrils without the presence of substrates in the organic phase. e) Fluorescence microscopy images and f) macroscopic photos showing the varied stability of Pickering emulsion (electrostatically stained with HPTS) in the presence of KIV nanofibrils and p-nitrophenol esters, where the emulsion showed higher stability when n ≥ 10. Scale bars: 10 μm.

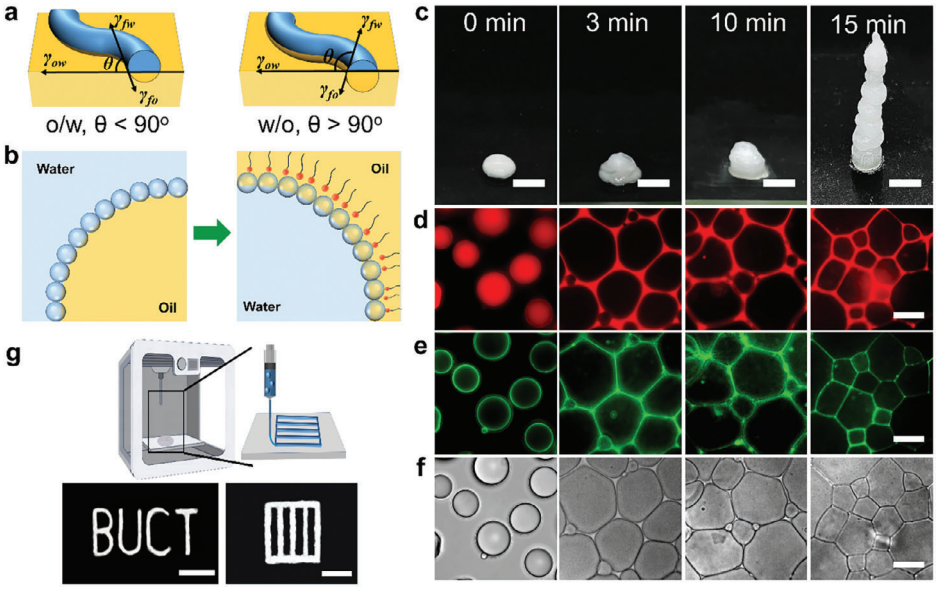

Figure 4. Emulsion evolution into HIPE gels. a) Schematic illustration showing colloid fibrils adsorbing at the oil–water interface. Left: hydrophilic fibrils ($\theta < 90°$) are less wetted by the oil phase, resulting in an o/w Pickering emulsion. Right: hydrophobic fibrils ($\theta > 90°$) exhibit greater wettability with the oil phase, forming a water-in-oil (w/o) Pickering emulsion. b) Interfacial catalysis leads to the generation of a surfactant layer that binds to the nanofibrils, facilitating phase inversion. c) Macroscopic images showing the evolution of chloroform/water (25:75) Pickering emulsion into HIPEs over time. After 15 min, a self-standing HIPE gel was achieved. d,e) Fluorescence and f) optical microscopic images showing the evolution of Pickering emulsion as the reaction proceeded. Nile red was dissolved in the oil phase, while ThT bound to cross-β-structure of amyloid nanofibrils. g) Extrusion-printed pattern with w/o HIPE gels. Scale bars: (c) 5 mm; (d–f) 10 µm; (g) 1.0 µm (left) and 0.2 µm (right).

laurate in the oil phase. After a designated incubation period and subsequent homogenization, the Pickering emulsion was thickened and a self-standing emulsion gel was obtained when the hydrolysis reaction was longer than 15 min (Figure 4c). Remarkably, the w/o Pickering emulsion was converted into HIPEs, characterized by an internal-phase volume fraction greater than 0.74,[24] in which water droplets were tightly trapped within the chloroform phase (Figure 4d–f). As the concentration of KIV nanofibrils increased, the spacing between aqueous pools decreased, leading to a morphological shift in water droplets from spherical to non-spherical shapes (Figure S20, Supporting Information). Notably, the o/w emulsion did not transform into w/o HIPE when the amyloid fibrils lacked catalytic residues (Figure S21, Supporting Information). Finally, we demonstrated direct 3D printing using the evolved HIPE gels into soft materials with designated shapes (Figure 4g).[25] Rheological measurements were conducted to evaluate the properties of the HIPE gels before and after printing, revealing a higher storage modulus compared to the loss modulus over a wide range of shear strains, which is characteristic of an elastic gel (Figure S22, Supporting Information). The results demonstrate that the HIPE gels exhibit shear-thinning behavior and recovery of strong elastic gelation after extrusion, making them well-suited for extrusion 3D printing.

2.4. Silicatein-Inspired Biomineralization within Emulsion Microcompartments

In nature, silicatein α is a serine hydrolase known for catalyzing the hydrolysis of silica precursors.[26] It is proposed that the hydrogen bond between the hydroxyl group of serine and the imidazole group of the histidine enhances the nucleophilicity of the serine residue, facilitating the hydrolysis of silanes such as tetraethoxysilane (TEOS, **Figure 5**a). This silicification mechanism serves as an excellent model for biomimetic inorganic material synthesis, due to its simple reaction pathway and mild conditions. Structurally, KIV contains both histidine and serine residues, enabling it to mimic the catalytic properties of silicatein. To test this hypothesis, we prepared a chloroform/water (3:7) Pickering emulsion using amyloid fibrils as the stabilizing agents, with chloroform as the internal organic phase and TEOS as the silica precursor (Figure 5b). The catalyzed hydrolysis of TEOS by amyloid fibrils resulted in the condensation of silica networks surrounding the aqueous phase under mild conditions (pH 7.5), as demonstrated by fluorescence microscopy and scanning electron microscopy (Figure 5c–e). This silicification process significantly improved the stability of the emulsion droplets, which maintained their spherical shape even after solvent evaporation (Figure 5d,e). Notably, the hydrolysis and condensation reaction occurred at pH 7.5 without the addition of ammonia or a strong base, which we attribute to the catalytic role of the histidine residue. The enhanced interfacial stability post-silicification was demonstrated through jamming/unjamming experiments (Figure 5f), while the solidification of the Pickering emulsion was confirmed by its self-standing nature and plasticity (Figure 5g and S23, Supporting Information).

3. Conclusion

In summary, we developed a Pickering emulsion system capable of evolving into microcompartments with enhanced stability and

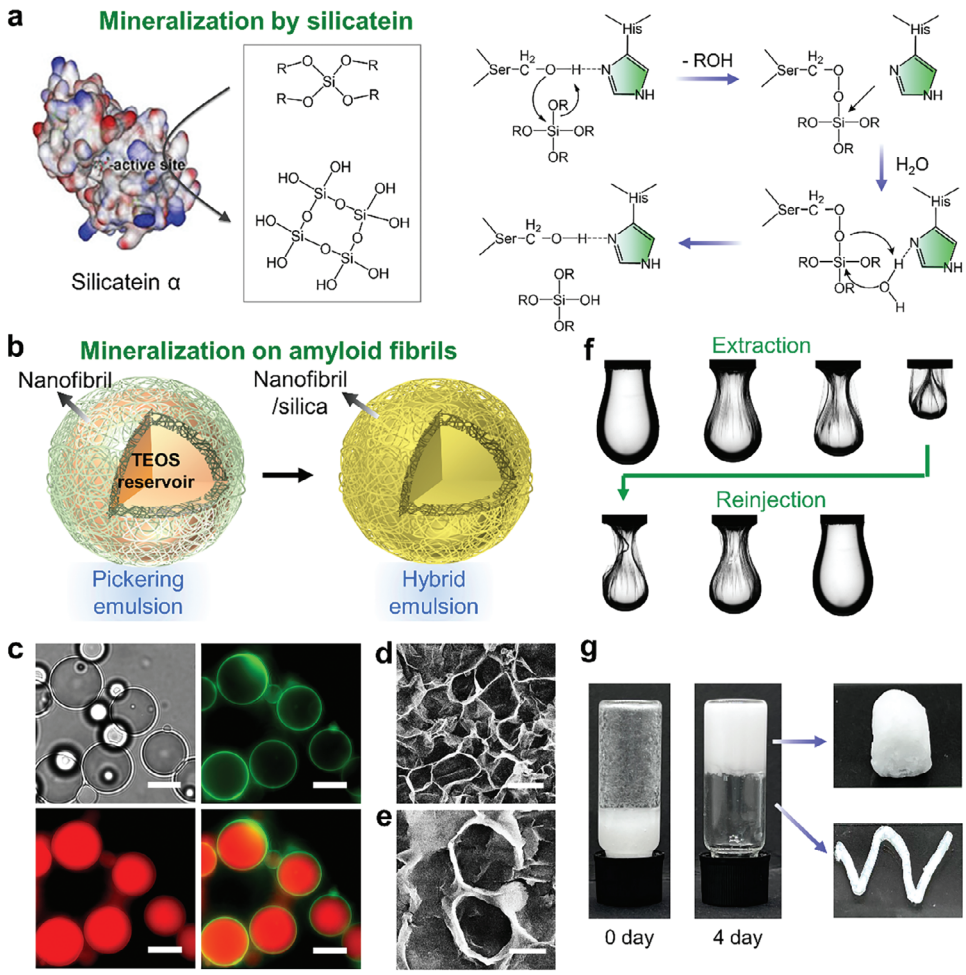

Figure 5. Self-strengthening of Pickering emulsion through silicatein-inspired biomineralization. a) Structure of silicatein *α* and its catalytic role in silane hydrolysis and subsequent condensation into silicate. Histidine and serine are key residues in this catalytic process. b) Schematic representation of biomineralization at the oil–water interface, catalyzed by amyloid nanofibrils, where TEOS was stored in the oil phase as a silica precursor. c) Optical and fluorescence microscopy showing the formation of a silica scaffold that stabilized the o/w Pickering emulsion. The interfacial silica layer was labeled with fluorescein isothiocyanate-conjugated 3-aminopropyltriethoxysilane (FITC-APTES), and the internal organic phase was stained with Nile red (red). d,e) Scanning electron microscopy (SEM) images showing the formation of hybrid microcompartments after silicification. f) The jamming/unjamming test demonstrates the formation of a solid film resulting from peptide-catalyzed silicification. g) Photos illustrating the transformation of the fluidic chloroform/water Pickering emulsion into self-standing emulsion gels following the catalytic hydrolysis and condensation of silica over a 4-day reaction period, enabling the creation of 3D objects. Scale bars: (c,d) 10 µm; (e) 15 µm.

complexity. Central to this design was a lipase-derived tridecapeptide that underwent amyloid fibrillation, resulting in supramolecular helical nanofibrils with hydrolase-like catalytic activity. The adsorption of these amyloid nanofibrils at the oil–water interface improved interfacial stability, enabling the formation of diverse Pickering emulsions across various organic solvents. Leveraging nanofibril-enabled biomimetic catalysis, the Pickering emulsion effectively converted ester substrates into amphiphilic fatty acids. This conversion generated a self-organized surfactant layer at the oil–water interface, leading to phase inversion and the subsequent formation of HIPE gels. Additionally, we implemented silicatein-inspired biomineralization to create silica networks that support the emulsion interface, further reinforcing the microcompartments. The design of these self-evolving soft materials holds promise for developing intelligent materials that mimic cellular behaviors observed in living organisms.

Supporting Information

Supporting Information is available from the Wiley Online Library or from the author.

Acknowledgements

The authors thank the National Natural Science Foundation of China (22172007, 32371525, T2221001, 92353304), the Science Fund for Creative Research Groups of the National Natural Science Foundation of China (52221006), the Strategic Priority Research Program of the Chinese Academy of Sciences (XDB37020105), the Fundamental Research Funds

for the Central Universities (buctrc202015) and the Open Research Fund Program of Cultivation Project of Double First-Class Disciplines of Light Industry Technology and Engineering, Beijing Technology & Business University (BTBU) for financial support.

Conflict of Interest

The authors declare no conflict of interest.

Data Availability Statement

The data that support the findings of this study are available in the supplementary material of this article.

Keywords

artificial cells, biomimetic chemistry, living materials, peptide self-assembly, pickering emulsion

Received: October 17, 2024
Revised: November 27, 2024
Published online: December 13, 2024

[1] S. Mann, *Angew. Chem., Int. Ed.* **2008**, *47*, 5306.
[2] a) S. Chen, Q. Guo, J. Yu, *Aggregate* **2022**, *3*, e293; b) M. E. Allen, J. W. Hindley, D. K. Baxani, O. Ces, Y. Elani, *Nat. Rev. Chem.* **2022**, *6*, 562; c) C. Guindani, L. C. da Silva, S. Cao, T. Ivanov, K. Landfester, *Angew. Chem., Int. Ed.* **2022**, *61*, 202110855.
[3] a) Y. Li, R. Tian, H. Shi, J. Xu, T. Wang, J. Liu, *Aggregate* **2023**, *4*, e317; b) X. Wang, X. Liu, X. Huang, *Adv. Mater.* **2020**, *32*, 2001436; c) K. A. Podolsky, N. K. Devaraj, *Nat. Rev. Chem.* **2021**, *5*, 676; d) M. Weiss, J. P. Frohnmayer, L. T. Benk, B. Haller, J.-W. Janiesch, T. Heitkamp, M. Börsch, R. B. Lira, R. Dimova, R. Lipowsky, E. Bodenschatz, J.-C. Baret, T. Vidakovic-Koch, K. Sundmacher, I. Platzman, J. P. Spatz, *Nat. Mater.* **2018**, *17*, 89; e) J. Li, W. D. Jamieson, P. Dimitriou, W. Xu, P. Rohde, B. Martinac, M. Baker, B. W. Drinkwater, O. K. Castell, D. A. Barrow, *Nat. Commun.* **2022**, *13*, 4125; f) B. Ghosh, R. Bose, T. Y. D. Tang, *Curr. Opin. Colloid Interface Sci.* **2021**, *52*, 101415.
[4] a) M. Marguet, L. Edembe, S. Lecommandoux, *Angew. Chem., Int. Ed.* **2012**, *51*, 1173; b) W. Mu, Z. Ji, M. Zhou, J. Wu, Y. Lin, Y. Qiao, *Sci. Adv.* **2021**, *7*, eabf9000; c) W.-C. Su, J. C. S. Ho, D. L. Gettel, A. T. Rowland, C. D. Keating, A. N. Parikh, *Nat. Chem.* **2024**, *16*, 54.
[5] E. Sokolova, E. Spruijt, M. M. K. Hansen, E. Dubuc, J. Groen, V. Chokkalingam, A. Piruska, H. A. Heus, W. T. S. Huck, *Proc. Natl. Acad. Sci. USA* **2013**, *110*, 11692.
[6] H. Li, Y. Yan, J. Chen, K. Shi, C. Song, Y. Ji, L. Jia, J. Li, Y. Qiao, Y. Lin, *Sci. Adv.* **2023**, *9*, eade5853.
[7] a) B. C. Buddingh', J. Elzinga, J. C. M. van Hest, *Nat. Commun.* **2020**, *11*, 1652; b) A. Dupin, F. C. Simmel, *Nat. Chem.* **2019**, *11*, 32; c) A. Samanta, V. Sabatino, T. R. Ward, A. Walther, *Nat. Nanotechnol.* **2020**, *15*, 914; d) S. Yang, A. Joesaar, B. W. A. Bögels, S. Mann, T. F. A. de Greef, *Angew. Chem., Int. Ed.* **2022**, *61*, 202202436.
[8] a) S. Yao, B. Jin, Z. Liu, C. Shao, R. Zhao, X. Wang, R. Tang, *Adv. Mater.* **2017**, *29*, 1605903; b) F. C. Meldrum, H. Cölfen, *Chem. Rev.* **2008**, *108*, 4332.
[9] a) K. Liu, A. Blokhuis, C. van Ewijk, A. Kiani, J. Wu, W. H. Roos, S. Otto, *Nat. Chem.* **2024**, *16*, 79; b) S. Panja, D. J. Adams, *Giant* **2021**, *5*, 100041.
[10] H. Chen, W. Li, Y. Lin, L. Wang, X. Liu, X. Huang, *Angew. Chem., Int. Ed.* **2020**, *59*, 16953.
[11] a) T. Aida, E. W. Meijer, S. I. Stupp, *Science* **2012**, *335*, 813; b) H. Wang, Z. Yang, D. J. Adams, *Mater. Today* **2012**, *15*, 500; c) J. Wang, K. Liu, R. Xing, X. Yan, *Chem. Soc. Rev.* **2016**, *45*, 5589; d) G. Wei, Z. Su, N. P. Reynolds, P. Arosio, I. W. Hamley, E. Gazit, R. Mezzenga, *Chem. Soc. Rev.* **2017**, *46*, 4661; e) C. Yuan, W. Ji, R. Xing, J. Li, E. Gazit, X. Yan, *Nat. Rev. Chem.* **2019**, *3*, 567; f) J. Zhang, Y. Wang, B. J. Rodriguez, R. Yang, B. Yu, D. Mei, J. Li, K. Tao, E. Gazit, *Chem. Soc. Rev.* **2022**, *51*, 6936; g) M. Zhu, J. Chen, Y. Lin, *Supramol. Mater.* **2023**, *2*, 100030; h) T. Jiang, C. Xu, Y. Liu, Z. Liu, J. S. Wall, X. Zuo, T. Lian, K. Salaita, C. Ni, D. Pochan, V. P. Conticello, *J. Am. Chem. Soc.* **2014**, *136*, 4300.
[12] a) Y. Song, U. Shimanovich, T. C. T. Michaels, Q. Ma, J. Li, T. P. J. Knowles, H. C. Shum, *Nat. Commun.* **2016**, *7*, 12934; b) S. Bai, C. Pappas, S. Debnath, P. W. J. M. Frederix, J. Leckie, S. Fleming, R. V. Ulijn, *ACS Nano* **2014**, *8*, 7005; c) Y. Nishida, A. Tanaka, S. Yamamoto, Y. Tominaga, N. Kunikata, M. Mizuhata, T. Maruyama, *Angew. Chem., Int. Ed.* **2017**, *56*, 9410; d) S. Mondal, M. Varenik, D. N. Bloch, Y. Atsmon-Raz, G. Jacoby, L. Adler-Abramovich, L. J. W. Shimon, R. Beck, Y. Miller, O. Regev, E. Gazit, *Nat. Commun.* **2017**, *8*, 14018.
[13] a) W. Zhang, B. P. Binks, J. Jiang, Z. Cui, *Angew. Chem., Int. Ed.* **2023**, *62*, 202310743; b) Y. Liu, H. Zhang, W. Zhang, B. P. Binks, Z. Cui, J. Jiang, *Angew. Chem., Int. Ed.* **2023**, *62*, 202210050; c) Z. Sun, C. Yang, F. Wang, B. Wu, B. Shao, Z. Li, D. Chen, Z. Yang, K. Liu, *Angew. Chem., Int. Ed.* **2020**, *59*, 9365.
[14] C. Wan, Y. Wu, Q. Cheng, X. Yu, Y. Song, C. Guan, X. Tan, C. Huang, J. Zhu, T. P. Russell, *J. Am. Chem. Soc.* **2023**, *145*, 25431.
[15] a) K. Li, H. Zou, R. Ettelaie, J. Zhang, H. Yang, *Angew. Chem., Int. Ed.* **2023**, *62*, 202300794; b) H. Jiang, L. Hong, Y. Li, T. Ngai, *Angew. Chem., Int. Ed.* **2018**, *57*, 11662; c) Z. Sun, X. Yan, Y. Xiao, L. Hu, M. Eggersdorfer, D. Chen, Z. Yang, D. A. Weitz, *Particuology* **2022**, *64*, 153; d) B. P. Binks, *Curr. Opin. Colloid Interface Sci.* **2002**, *7*, 21; e) X. Zhang, Y. Hou, R. Ettelaie, R. Guan, M. Zhang, Y. Zhang, H. Yang, *J. Am. Chem. Soc.* **2019**, *141*, 5220; f) C. A. Zentner, F. Anson, S. Thayumanavan, T. M. Swager, *J. Am. Chem. Soc.* **2019**, *141*, 18048; g) Z. Sun, U. Glebe, H. Charan, A. Böker, C. Wu, *Angew. Chem., Int. Ed.* **2018**, *57*, 13810.
[16] Y. Ming, Y. Xia, G. Ma, *Aggregate* **2022**, *3*, e162.
[17] J. Chen, K. Shi, R. Chen, Z. Zhai, P. Song, L. W. Chow, R. Chandrawati, E. T. Pashuck, F. Jiao, Y. Lin, *Angew. Chem., Int. Ed.* **2024**, *63*, 202317887.
[18] Q. Xu, Y. Ma, Y. Sun, D. Li, X. Zhang, C. Liu, *Aggregate* **2023**, *4*, e333.
[19] a) O. Zozulia, M. A. Dolan, I. V. Korendovych, *Chem. Soc. Rev.* **2018**, *47*, 3621; b) Y. Maeda, N. Javid, K. Duncan, L. Birchall, K. F. Gibson, D. Cannon, Y. Kanetsuki, C. Knapp, T. Tuttle, R. V. Ulijn, H. Matsui, *J. Am. Chem. Soc.* **2014**, *136*, 15893; c) A. Chatterjee, A. Reja, S. Pal, D. Das, *Chem. Soc. Rev.* **2022**, *51*, 3047; d) X. Huang, X. Liu, Q. Luo, J. Liu, J. Shen, *Chem. Soc. Rev.* **2011**, *40*, 1171; e) G. Gulseren, M. A. Khalily, A. B. Tekinay, M. O. Guler, *J. Mater. Chem. B* **2016**, *4*, 4605; f) Y. Wang, L. Yang, M. Wang, J. Zhang, W. Qi, R. Su, Z. He, *ACS Catal.* **2021**, *11*, 5839; g) M. O. Guler, S. I. Stupp, *J. Am. Chem. Soc.* **2007**, *129*, 12082; h) A. Singh, S. Goswami, P. Singh, D. Das, *Angew. Chem., Int. Ed.* **2023**, *62*, 202315716; i) G. Ashkenasy, M. Samanta, N. Saad, D. Wu, N. S. A. Crone, K. Abramov-Harpaz, C. Regev, R. Cohen-Luria, A. L. Boyle, Y. Miller, A. Kros, *Angew. Chem., Int. Ed.* **2024**, 202413810; j) S. Roy, J. Laha, A. Reja, D. Das, *J. Am. Chem. Soc.* **2024**, *146*, 22522.
[20] P. S. P. Wang, J. B. Nguyen, A. Schepartz, *J. Am. Chem. Soc.* **2014**, *136*, 6810.
[21] R. Aveyard, B. P. Binks, J. H. Clint, *Adv. Colloid Interface Sci.* **2003**, *100–102*, 503.
[22] M. D. Nothling, Z. Xiao, A. Bhaskaran, M. T. Blyth, C. W. Bennett, M. L. Coote, L. A. Connal, *ACS Catal.* **2019**, *9*, 168.

[23] a) B. Wang, B. Yin, Z. Zhang, Y. Yin, Y. Yang, H. Wang, T. P. Russell, S. Shi, *Angew. Chem., Int. Ed.* **2022**, *61*, 202114936; b) H. Sun, L. Li, T. P. Russell, S. Shi, *J. Am. Chem. Soc.* **2020**, *142*, 8591.
[24] a) K. Kim, S. Kim, J. Ryu, J. Jeon, S. G. Jang, H. Kim, D.-G. Gweon, W. B. Im, Y. Han, H. Kim, S. Q. Choi, *Nat. Commun.* **2017**, *8*, 14305; b) D. Li, H. Yin, Y. Wu, W. Feng, K.-f. Xu, H. Xiao, C. Li, *J. Agric. Food Chem.* **2023**, *71*, 18829; c) V. O. Ikem, A. Menner, A. Bismarck, **2008**, *47*, 8277.
[25] Z. Lin, X. Qiu, Z. Cai, J. Li, Y. Zhao, X. Lin, J. Zhang, X. Hu, H. Bai, *Nat. Commun.* **2024**, *15*, 4806.
[26] M. A. A. Abdelhamid, S. P. Pack, *Acta Biomater.* **2021**, *120*, 38.

